

# Striped Ultradilute Liquid of Dipolar Bosons in Two Dimensions

Clemens Staudinger<sup>1</sup>, Diana Hufnagl<sup>2,3</sup>, Ferran Mazzanti<sup>4</sup> and Robert E. Zillich<sup>1</sup>

<sup>1</sup>*Institute for Theoretical Physics, Johannes Kepler University, Altenbergerstrasse 69, 4040 Linz, Austria*

<sup>2</sup>*Johann Radon Institute for Computational and Applied Mathematics,  
Austrian Academy of Sciences, Altenberger Straße 69, 4040 Linz, Austria*

<sup>3</sup>*MathConsult GmbH, Altenbergerstrasse 69, Linz, Austria*

<sup>4</sup>*Departament de Física, Campus Nord B4-B5, Universitat Politècnica de Catalunya, E-08034 Barcelona, Spain*

We investigate the phases of a Bose-Einstein condensate of dipolar atoms restricted to move in a two-dimensional plane. The dipole moments are all aligned in a direction tilted with respect to the plane normal. As a result of the attractive and repulsive components of the dipole-dipole interaction, the dipolar gas has a self-bound phase, which is stabilized by quantum fluctuations. Furthermore, tilting the dipoles tunes the anisotropy of the dipole-dipole interaction, which can trigger a spatial density modulation. In this work we study these two aspects and investigate the conditions for the formation of a self-bound and striped phase, which has been realized in experiments with dipolar droplets. We use a variational method based on the hypernetted-chain Euler-Lagrange optimization of a Jastrow-Feenberg ansatz for the many-body wave function to study the ground state properties. This method takes into account quantum fluctuations in a non-perturbative way and thus can be used also for strongly correlated systems.

## I. INTRODUCTION

Dipolar quantum gases, and especially dipolar Bose-Einstein condensates (BEC), are gaining again significant attention [1] since self-bound droplets consisting of <sup>164</sup>Dy [2–7] and <sup>166</sup>Er [8] were realized in experiments. In contrast to Bose mixtures, the competition between attractive and repulsive parts of the interaction does not originate from the interaction between the components of the mixture, but rather from the dipole-dipole interaction itself, which in general has repulsive and attractive regions. As in Bose mixtures droplets, quantum fluctuations are the driving force behind the stabilization of dipolar droplets, as confirmed by theory [9–11]. More recently, even droplets consisting of dipolar mixtures have been realized in experiments [12, 13] and described with beyond mean-field methods [14, 15]. In such droplets the components are not necessarily miscible, but can demix while staying self-bound.

In experiments the dipole moments of all atoms are aligned in parallel by an external magnetic field of well-controlled strength and direction. This provides a means to modify the anisotropy of the dipole-dipole interaction and triggers the transition to a density-modulated, self-organized stripe phase, which shows supersolid properties [16–21]. Such a transition is also visible in the excitation spectrum of a dipolar BEC, where a so-called roton minimum emerges [22–27]. Just like a droplet, a density modulation is a state that is not stable in a mean-field approximation [28], but rather stabilized by quantum fluctuations [29].

In previous theoretical studies [30] we observed density modulations in the form of stripes in a two-dimensional dipolar Bose gas with the polarization axis tilted with respect to the perpendicular direction. In these studies, where the tilt angle  $\theta$  was small enough that the dipole interaction stayed purely repulsive, a very high density was required to reach the stripe phase, and no self-binding

was involved. In this work we investigate the formation of stripes at much lower densities which can be realized in experiments with magnetic dipole moments. We achieve this by increasing the tilting angle  $\theta$  beyond a critical angle, where the projection of the dipole-dipole interaction on the 2D plane becomes attractive, see fig. 1, such that self-binding is possible. Density oscillations were observed experimentally [31–34]. Conventional mean-field theories are not capable of describing such situations, and more powerful methods like extended mean-field with Lee-Huang-Yang corrections [5, 8], or Quantum Monte Carlo (QMC) techniques [11, 35–38] have to be applied. In this work we employ the hypernetted-chain Euler-Lagrange (HNC-EL) method [39–41], which incorporates correlations beyond mean-field approaches especially for strongly-correlated and self-bound systems [42, 43] and requires a much lower computational effort than QMC.

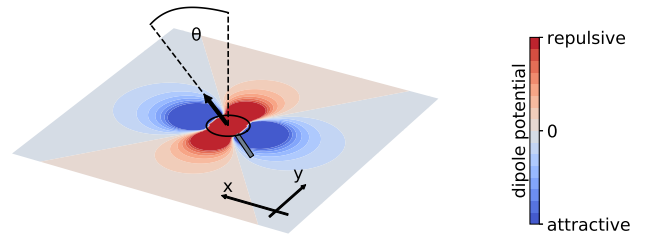


FIG. 1. Sketch of the dipolar interaction in 2D, with tilting angle  $\theta$  and hard core parameter  $C_h$ . The direction of the dipole moment is shown by the black arrow and the hard core is implied by the black circle. The repulsive and attractive regions of the compound interaction are shown with red and blue colors, respectively.

## II. METHODOLOGY

In the following we consider a dipolar Bose gas that is so tightly trapped in the  $z$ -direction that we can assume particles are restricted to move in two dimensions, taken to be the  $xy$ -plane. The Hamiltonian reads

$$\hat{H} = -\frac{\hbar^2}{2m} \sum_{i=1}^N \Delta_i + \sum_{i<j} v(\mathbf{r}_i - \mathbf{r}_j), \quad (1)$$

with the interaction being the sum of the dipolar term and a repulsive core

$$v(\mathbf{r}) = \frac{C_{dd}}{4\pi} \left[ \frac{1}{|\mathbf{r}|^3} - \frac{3(x \sin \theta)^2}{|\mathbf{r}|^5} \right] + \frac{E_0 C_h^{12}}{|\mathbf{r}|^{12}}. \quad (2)$$

In this expression  $C_{dd}$  sets the strength of the dipolar interaction and is proportional to the square of the (electric or magnetic) dipole moment. It is useful to define the characteristic length scale  $r_0 = mC_{dd}/(4\pi\hbar^2)$  and the associated energy scale  $E_0 = \hbar^2/(mr_0^2)$ , which serve as units for our calculations. All dipoles are polarized along a direction in the  $xz$ -plane that forms an angle  $\theta$  with respect to the  $z$ -axis, see Fig. 1. With this geometry, the dipole-dipole interaction is repulsive around the  $y$ -direction (red regions in fig. 1), but for large enough  $\theta > \theta_c = \arcsin(1/\sqrt{3}) \approx 0.61548$  an attractive region appears in the  $x$ -direction (blue regions in fig. 1). In this work we explore the highly tilted polarization regime  $\theta > \theta_c$  where the purely dipolar gas is unstable. In order to prevent collapse, we add a short range repulsive interaction  $C_h/r^{12}$ -potential with the short-range repulsion parameter  $C_h$  as shown in Eq. (2). As a check of universality of this model we compare the results with those obtained with a  $1/r^6$ -potential.

We describe the ground state using a variational Jastrow-Feenberg ansatz [44] of the form

$$\Psi(\mathbf{r}_1, \dots, \mathbf{r}_N) = \exp \left[ \frac{1}{2} \sum_{i<j} u(\mathbf{r}_i - \mathbf{r}_j) \right], \quad (3)$$

which includes pair correlations  $u(\mathbf{r})$  and accounts for quantum fluctuations. To obtain the optimal ground state we solve the Euler-Lagrange equation

$$\frac{\delta e}{\delta \sqrt{g(\mathbf{r})}} = 0 \quad (4)$$

where  $e$  is the energy per particle

$$e(\rho_0) \equiv \frac{E}{N} = \frac{\rho_0}{2} \int d^2r g(\mathbf{r}) \left[ v(\mathbf{r}) - \frac{\hbar^2}{4m} \nabla^2 u(\mathbf{r}) \right]. \quad (5)$$

The pair distribution function  $g(\mathbf{r})$  is given in terms of the wave function in Eq. (3) as

$$g(\mathbf{r}_1 - \mathbf{r}_2) = \frac{N(N-1)}{\langle \Psi | \Psi \rangle \rho_0^2} \int d^2r_3 \dots d^2r_N |\Psi(\mathbf{r}_1, \dots, \mathbf{r}_N)|^2, \quad (6)$$

Closure is provided by the HNC relation between  $g(\mathbf{r})$  and  $u(\mathbf{r})$  [45]. In the following we restrict ourselves to the HNC-EL/0 approximation, where the so-called elementary diagrams are neglected in the cluster expansion [45]. We have calculated the leading contribution of the elementary diagrams to the total energy but found it to be less than 3% for densities  $\rho_0 r_0^2 \leq 1$  (see appendix C). In the HNC-EL/0 framework, Eq. (4) can be cast as

$$\left[ -\frac{\hbar^2}{m} \Delta + v(\mathbf{r}) + w_1(\mathbf{r}) \right] \sqrt{g(\mathbf{r})} = 0 \quad (7)$$

which has the form of an effective 2-body zero-energy scattering equation with the bare potential  $v$  and an additional induced many-body potential  $w_1$ , which is defined via its Fourier transform

$$w_1(\mathbf{k}) = -\frac{\hbar^2 k^2}{4m} \left( 1 - \frac{1}{S(\mathbf{k})} \right)^2 (2S(\mathbf{k}) + 1)$$

in terms of the static structure factor

$$S(\mathbf{k}) = 1 + \text{FT} [g(\mathbf{r}) - 1] \quad (8)$$

where FT denotes the Fourier transformation multiplied with the density  $\rho_0$ . We note that Eq.(7) is not a simple linear differential equation because the induced potential  $w_1$  depends on  $g$  itself. The details on how to solve Eq. (7) iteratively can be found elsewhere [40, 41].

From experience with other systems [42, 43, 46–48], solving the HNC-EL/0 equations is straightforward for systems with a stable or metastable ground state, but fails to converge if the system is unstable against infinitesimal perturbations (e.g. spinodal instability of a system with homogeneous density [43, 47]). Inspection of structural quantities like  $g(\mathbf{r})$  and  $S(\mathbf{k})$  provides clues as to the nature of the instability (e.g. long-ranged fluctuations in  $g(\mathbf{r})$  in the case of a spinodal instability). More quantitative information on that is provided by a stability analysis of the solution of the HNC-EL/0 equation [49]. For this purpose, we evaluate the second functional derivative of the energy  $e$  with respect to the pair distribution function,  $K(\mathbf{r}, \mathbf{r}') = \delta^2 e / \delta \sqrt{g(\mathbf{r})} \delta \sqrt{g(\mathbf{r}')}$ . If this operator is positive definite, the solution of the HNC-EL/0 equation (4) is stable against infinitesimal perturbations of  $g(\mathbf{r})$ . This is guaranteed if all eigenvalues  $\lambda_i$  in the equation

$$\int d^2r' K(\mathbf{r}, \mathbf{r}') f_i(\mathbf{r}') = \lambda_i f_i(\mathbf{r}) \quad (9)$$

are positive. Conversely, if the lowest eigenvalue  $\lambda_0$  is close to zero, the system approaches an instability. More importantly, the eigenvector  $f_0(\mathbf{r})$  provides information about the nature of the instability as shown by our results below. The explicit form of  $K(\mathbf{r}, \mathbf{r}')$  is easily calculated in the HNC-EL/0 approximation. Following the notation of Ref. [49], the eigenvalue problem can be written as

$$\left[ -\frac{\hbar^2}{m} \Delta + v(\mathbf{r}) + w_1(\mathbf{r}) + \hat{W} \right] f_i(\mathbf{r}) = \lambda_i f_i(\mathbf{r}) \quad (10)$$

where the  $\hat{W}$  operator is defined as

$$\hat{W}f_i(\mathbf{r}) = \rho_0 \int d^2r' \sqrt{g(\mathbf{r})}W(\mathbf{r} - \mathbf{r}')\sqrt{g(\mathbf{r}')}f_i(\mathbf{r}') \quad (11)$$

$W$  is given in momentum space as

$$W(\mathbf{k}) = -\frac{\hbar^2 k^2}{m} \left(1 - \frac{1}{S(\mathbf{k})^3}\right).$$

Since we only need the lowest eigenvalue to assess the stability, we solve eq.(10) by imaginary time propagation, see appendix A for details.

### III. ENERGY AND STABILITY

In the liquid phase, as opposed to the gas phase, a system is self-bound: the energy per particle is negative and attains its minimum at an equilibrium density  $\rho_{\text{eq}}$ . Furthermore, below the spinodal density a homogeneous liquid becomes unstable against long wavelength density fluctuations, and then breaks into droplets. In this section we analyze the ground state energy for various short range repulsion strengths  $C_h$ , dipole tilt angles  $\theta$  and densities  $\rho_0$  in order to check whether the system is in a liquid or in a gas phase. We also assess the stability against density fluctuations. Instead of reaching a spinodal instability typical of isotropic liquids, we find a transition to a density wave in the  $y$ -direction, i.e. a stripe phase.

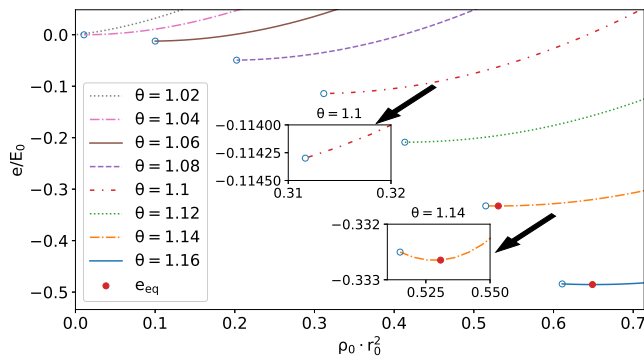


FIG. 2. Energy per particle  $e(\rho_0)$  as a function of the density  $\rho_0$  for  $C_h = 0.33r_0$  and  $\theta = 1.02 - 1.16$ . The last converging point at the lowest density in each curve is marked with a blue open circle and the equilibrium energy  $e_{\text{eq}}$  with a red filled circle. The insets show a magnification of the result for  $\theta = 1.10$  and  $1.14$ , which illustrate the behavior of the equation of state near the stripe phase.

We first fix  $C_h = 0.33r_0$  and vary the tilt angle between  $\theta = 1.02$  and  $\theta = 1.16$ . The results are depicted in fig. 2, where we show the energy per particle  $e(\rho_0)$  as a function of the density. In each case we start the calculation at the largest density considered and solve Eq. (4) iteratively. The resulting pair distribution function is then used as an

input to solve the same equation at the next lower density in the grid. This procedure ensures rapid convergence. Depending on the tilting angle  $\theta$  three different cases can occur, corresponding to three different phases: a gas, a homogeneous liquid, or a striped liquid.

For  $\theta \leq 1.04$  the energy per particle is positive and approaches zero as  $\rho \rightarrow 0$  where it attains its minimum value  $e = 0$ . The system is then in a gas phase and the corresponding pressure is always positive. Beyond  $\theta = 1.04$  the system enters a different phase where the energy becomes negative as the density is lowered. The system is self-bound and thus in a liquid phase. However, as long as  $\theta \leq 1.12$ , the calculation ceases to converge before the energy per particle attains a minimum; the density  $\rho_c$  where this happens is indicated with open blue circles in fig. 2. The inset for  $\theta = 1.1$  shows this more clearly, where one can see that the liquid phase stops being stable before reaching a homogeneous equilibrium density  $\rho_{\text{eq}}$ . The homogeneous HNC-EL/0 equations are known to cease to converge at a continuous phase transition [30, 43]. In the following we show that the dipolar system undergoes a transition to a self-organized stripe phase where the density exhibits a spatial modulation.

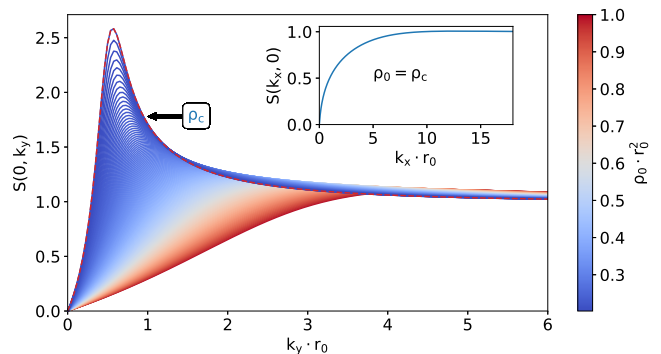


FIG. 3. Static structure factor  $S(0, k_y)$  for  $\theta = 1.08$  and  $C_h = 0.33r_0$  as a function of  $k_y$ . As the density (color coded) is lowered approaching a critical density  $\rho_c = 0.2023/r_0^2$ , a large peak develops.  $S(k_x, 0)$ , shown in the inset, is almost independent on  $\rho_0$  and does not develop a peak.

Fig. 3 shows the static structure factor  $S(k_x = 0, k_y)$  along the  $y$ -direction, for  $\theta = 1.08$  and  $C_h = 0.33r_0$ , and densities spanning the range from  $0.2023/r_0^2$  to  $1/r_0^2$ . A pronounced peak appears when the density approaches a critical value  $\rho_c = 0.2023/r_0^2$ , thus signaling increasing spatial order in that direction. This suggests a self-organized long-range order below  $\rho_c$ , where homogeneous HNC-EL/0 does not converge anymore, as it happened for tilted dipoles in Ref. [30], except that here the density is three orders of magnitude lower and the dipoles are in a self-bound phase. From the position  $k_p$  of the peak in  $S(k_x = 0, k_y)$  at  $\rho_c$  we can predict the wave number of the density oscillation. In contrast, the structure factor in  $x$ -direction has no peak at all (see inset in fig. 3), thus showing no signs of ordering in  $x$ -direction. Figure 4

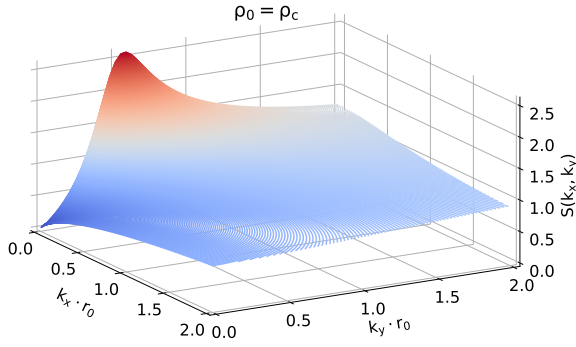


FIG. 4. Static structure factor  $S(k_x, k_y)$  for  $\theta = 1.08$ ,  $C_h = 0.33r_0$  at the critical density  $\rho_c = 0.2023/r_0^2$ .

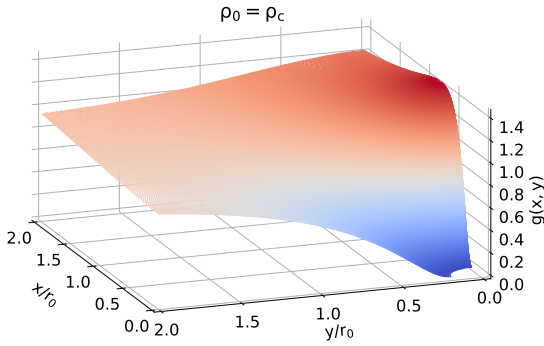


FIG. 5. Pair distribution function  $g(x, y)$  for  $\theta = 1.08$ ,  $C_h = 0.33r_0$  at the critical density  $\rho_c = 0.2023/r_0^2$ .

shows the full  $S(k_x, k_y)$  at the critical density  $\rho_c$ .

Fig. 5 shows the corresponding pair distribution function  $g(x, y)$  obtained as the Fourier transform of  $S(k_x, k_y)$ . As expected  $g(x, y)$  shows a small peak along the  $x$  direction where the attractive well of the dipole-dipole interaction (fig. 1) is deepest. Other than that, the pair distribution function is anisotropic but smooth. In the small range depicted,  $g(x, y)$  has little structure along the  $y$ -direction, and the fluctuations in  $g(0, y)$  that lead to the peak in  $S(0, k_y)$  cannot be seen.

The emergence of a peak in the static structure factor along the  $y$ -direction is already a strong indicator for the transition to a stripe phase. The more rigorous stability analysis explained above leads to the same conclusion, as illustrated in fig. 6. The top, middle and bottom panels correspond to  $(C_h = 0.33r_0, \theta = 1.08)$ ,  $(C_h = 0.33r_0, \theta = 1.16)$  and  $(C_h = 0.28r_0, \theta = 1.19)$ , respectively. The left panels depict the density dependence of the lowest eigenvalue  $\lambda_0$  of Eq.(10). As can be seen,  $\lambda_0$  approaches zero as the density approaches  $\rho_c$ , confirming that the homogeneous phase becomes unstable in that limit. As a further confirmation we show the lowest eigenvectors  $f_0(\mathbf{r})$  in the right column of of the same figure. The shape of  $f_0$  informs about the least stable fluctuation in  $g(x, y)$ , which drives the transition to a stripe phase, showing

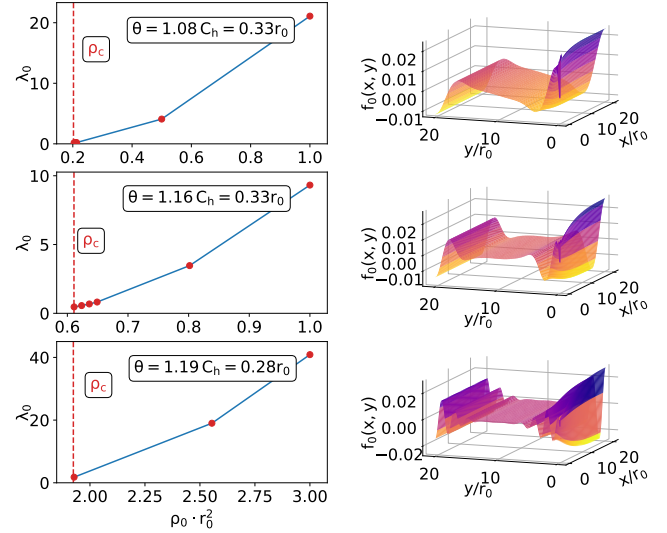


FIG. 6. Stability analysis for  $C_h = 0.33r_0$ ,  $\theta = 1.08/1.16$  and  $C_h = 0.28r_0$ ,  $\theta = 1.19$ . The left column shows the lowest eigenvalue  $\lambda_0$  of the Hessian as a function of the density  $\rho_0$ , while the right column shows the eigenvector  $f_0(\mathbf{r})$  at  $\rho_c$ .

oscillations along the  $y$ -direction. These oscillations are most pronounced at high densities, as seen in the bottom panel of the figure. The wave length corresponds to the location of the peak in  $S(0, k_y)$  at  $\rho = \rho_c$ , see Fig. 3. The wave number of this oscillation is the same as the wave number of the peak in  $S(0, k_y)$  for  $\rho_c$  (see fig. 3). This behavior clearly signals the transition to a phase with long range order in the  $y$ -direction. Note that in all cases, the oscillation is strongly damped, which was not found for the stripe phase transition at high densities in Ref. [30], where the system is not self-bound.

When the tilting angle is increased beyond  $\theta = 1.12$  while still keeping  $C_h = 0.33r_0$ , the energy decreases further due to the stronger attraction, but there is also a qualitative change of the shape of the equation of state:  $e(\rho_0)$  is not monotonous anymore, but reaches a minimum at a homogeneous equilibrium density  $\rho_{eq}$  before reaching the critical density  $\rho_c$  of the transition to the stripe phase. This new minimum corresponds to a self-bound homogeneous liquid state. If the system were finite, the dipoles would form a two-dimensional droplet adjusting its radius so that the pressure inside the droplet is zero at  $\rho_{eq}$ . When the density is lowered further the energy per particle starts increasing again, up to the point where the transition to the stripe phase takes place at  $\rho_c$ , as evidenced by the stability analysis shown in fig. 6). The lower inset in fig. 2 shows the result for  $\theta = 1.14$ , where the energy minimum at  $\rho_{eq}$  is clearly visible.

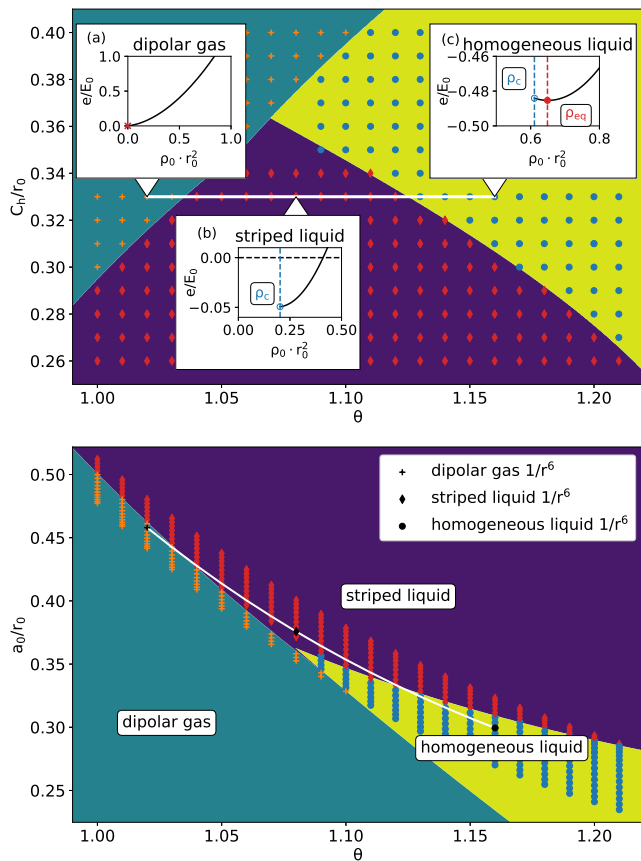


FIG. 7. Phase diagram as a function of the tilting angle  $\theta$  and short-range repulsion  $C_h$  (upper panel) and as a function of the scattering length  $a_0$  (lower panel). The insets (a), (b), and (c) show a representative  $e(\rho_0)$  for each phase for  $\theta = 1.02, 1.08$ , and  $1.16$ , respectively, all for the same value of  $C_h = 0.33r_0$  (white line). In the lower panel the three black symbols show the result of a calculation with a  $1/r^6$ -repulsion, which gives the same result as the  $1/r^{12}$ -repulsion used for all other calculations.

#### IV. PHASE DIAGRAM

In order to obtain the full phase diagram, we calculate  $e(\rho_0)$  for a wide range of  $\theta$  and  $C_h$  values following the protocol described above, i.e. lowering  $\rho_0$  from a sufficiently large value down to zero or until a homogeneous phase ceases to be stable at a finite density value  $\rho_c$ . We analyze the results in the same way as in the previous section to classify the phase into gas, striped liquid, and homogeneous liquid. In fig. 7 we indicate the phase by different colors. The lower panel of fig. 7 depicts the same phase diagram as the upper panel, but in terms of the scattering length  $a_0$  of the interaction (2) instead of  $C_h$  to make it independent of the interaction [50]. The scattering length  $a_0$  depends on both  $C_h$  and  $\theta$ , and increasing  $C_h$  decreases  $a_0$ , see fig. 8. We also include three points, marked in black, corresponding to

an interaction  $1/r^6$  but tuned to give the same scattering length of the compound system. These calculations give the same phase as those with the  $1/r^{12}$ -repulsion, which indicates a universal behavior that is independent of the details of the short-range interaction beyond its scattering length. Based on the shown grid of  $\theta$  and  $C_h$  values, the boundaries between the phases were calculated using a C-support vector machine [51], and an analytic expression for those phase boundaries is given in appendix B. In the upper panel of fig. 7 a white line is drawn for the fixed repulsion parameter  $C_h = 0.33r_0$  that we used in the previous section. The three insets show three examples for the equation of state  $e(\rho_0)$  along this line, each representing one of the phases. The points along the white line are the results of the energies  $e(\rho_0)$  discussed earlier in fig. 2. Note, that a dipolar system in 2D can still have a density oscillation at densities  $\rho_0 \sim 10^2/r_0^2$  as shown in [30]. However, here we focus on the formation of a stripe phase at orders of magnitude lower densities.

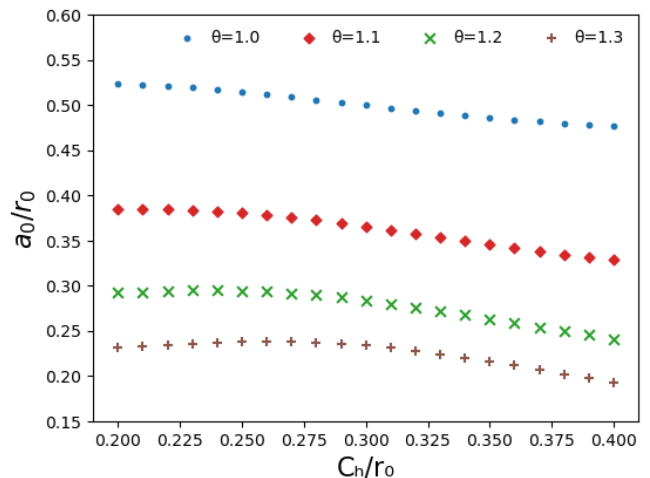


FIG. 8. Scattering length  $a_0$  of the interaction (2) as function of the repulsion parameter  $C_h$  for 4 different tilting angles  $\theta$ .

Fig. 7 shows that, for tilting angle  $\theta > 1.07$ , upon increasing the strength  $C_h$  of the repulsion the system undergoes first a transition from a striped liquid to a homogeneous liquid, and then a transition to a homogeneous gas. The reason is that the increasing isotropic short-range repulsion becomes dominant compared to the anisotropic dipole-dipole interaction, which is responsible for the formation of stripes. More interestingly, an increase of the tilting angle  $\theta$ , and thus of the anisotropy, for a fixed short-range interaction, also drives the system to the homogeneous liquid phase, as we have discussed in Sec. III. This might seem counter-intuitive at first. However, it is actually the repulsive part of the dipole-dipole interaction in  $y$ -direction causing the formation of stripes and this part of the interaction does not change with  $\theta$ . At the same time the attraction in  $x$ -direction increases with increasing  $\theta$  and leads to a more strongly bound

system with a higher density, and the stripes merge as their wave length decreases. For example if  $C_h = 0.33r_0$  is fixed and the tilting angle is increased from  $\theta = 1.08$  to  $\theta = 1.16$  the wave length decreases from  $\lambda = 11.70r_0$  to  $\lambda = 4.82r_0$ .

In the lower panel of fig. 7 we characterize the phase diagram using the scattering length  $a_0$  of the full interaction instead of the short-range repulsion parameter  $C_h$ . This way, the phase diagram becomes more intuitive: for a given  $a_0$ , the system undergoes a transition from an homogeneous liquid to a striped liquid phase with increasing  $\theta$ .

## V. CRITICAL DENSITY

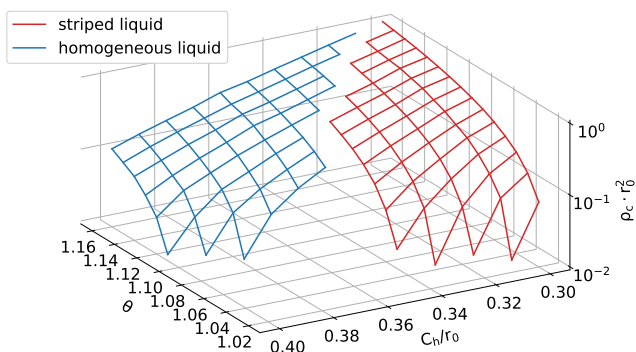


FIG. 9. Critical density  $\rho_c$  for the transition to the stripe phase as a function of  $\theta$  and  $C_h$ . The red and blue surfaces denote the regimes of striped liquid and homogeneous liquid, respectively, see fig. 7. At the border to the gas phase,  $\rho_c$  falls to zero.

Figure 9 shows the critical density  $\rho_c$  for the transition to a stripe phase as a function of tilting angle  $\theta$  and repulsion strength  $C_h$ , showing that  $\rho_c$  increases with increasing  $\theta$  and decreasing  $C_h$ . The blue and red surfaces represent the regions of the homogeneous liquid and the striped liquid, respectively. Both surfaces approach  $\rho_c = 0$  as the system approaches the gas phase, seen as a sharp drop on the logarithmic scale in fig. 9. This shows that with a proper choice of  $\theta$  and  $C_h$  (or  $a_0$ ), stripes can be observed in arbitrarily dilute systems. This is markedly different from previous theoretical studies of tilted dipoles in two dimensions [30], where the dipole orientation was not tilted above  $\theta = \arcsin(1/\sqrt{3})$  such that the dipole-dipole interaction stays purely repulsive. In that case a stripe phase was predicted only above a critical density  $\rho_c = O(10^2)$ . We also note that in the range of  $\theta$  and  $C_h$  explored in this work,  $\rho_c r_0^2 < 1$ . Despite the variational nature of the calculations presented, the contribution of elementary diagrams to the energy per particle is less than 3% (see appendix C for details), while three- or higher-order correlations are negligible in the low density regime considered.

## VI. CONCLUSION

In this work we have explored the phase diagram of a dipolar gas in two dimensions as a function of the dipole tilting angle and their short-range repulsion. We have found that this system exhibits three different phases: a gas phase, a self-bound stripe phase, and a homogeneous self-bound stripeless phase. We detected the transition to a stripe phase by monitoring a peak that emerges in the structure factor close to a critical density  $\rho_c$  that marks the phase transition. The critical density depends on the short range repulsion and the tilting angle, and can be low enough so that it can be realized with current experimental setups. To further confirm the emergence of the low density stripe phase we have also conducted a stability analysis based on the Hessian of the energy. Although our calculations, based on the variational HNC-EL/0 method, always assumed homogeneity, this provides strong evidence that a self-bound and striped droplet can form in a two-dimensional anisotropic dipolar Bose gas.

In order to calculate the properties of the stripe phase one can use a variational model that allows for density modulations. This can be achieved with the inhomogeneous generalization of the HNC-EL method [52], which has been used for example to describe dipolar systems in quasi-2D geometries [53, 54]. Alternatively one can use exact diffusion Monte Carlo methods that are able to describe the system also in the stripe phase, using the optimal HNC-EL solutions as an ingredient for the guiding wave function. We are currently working along this line, in an attempt to study the self-bound nature of two-dimensional striped dipolar systems.

## ACKNOWLEDGMENTS

We acknowledge discussions with Jürgen T. Drachta and Tilman Pfau. F. Mazzanti acknowledges financial support by grant PID2020-113565GB-C21 funded by MCIN/AEI/10.13039/501100011033, and from Secretaria d'Universitats i Recerca del Departament d'Empresa i Coneixement de la Generalitat de Catalunya, co-funded by the European Union Regional Development Fund within the ERDF Operational Program of Catalunya (project QuantumCat, ref. 001-P-001644).

## Appendix A: Stability Analysis

Solving for the lowest eigenvalue  $\lambda_0$  and associated eigenvector  $y_0(x, y)$  of Eq. (10) can be done in several ways. Here we use imaginary time propagation

$$f_0 = \lim_{t \rightarrow \infty} \exp \left[ -t \left( -\frac{\hbar^2}{m} \Delta + v(\mathbf{r}) + w_I(\mathbf{r}) + \hat{W} \right) \right] \tilde{f} \quad (\text{A1})$$

where  $\tilde{f}$  is an initial guess with the only requirement that it has a non-zero projection onto  $f_0$ . As usual, the time propagation is split into small time steps  $\tau$  such that the exponentiation can be approximated in a suitable way. Here we use the Trotter approximation [55]. Taking the exponent of the potential functions  $v(\mathbf{r})$  and  $w_I(\mathbf{r})$  is trivial in  $r$ -space, while the exponential of the kinetic part is carried out in momentum space. However, the integral operator  $\hat{W}$  cannot be easily exponentiated. We could take the further approximation,  $\exp[-\tau\hat{W}] \approx 1 - \tau\hat{W}$ , but this would require an extremely small time step  $\tau$ . Therefore, we split the integration kernel in (11) as  $\hat{W} = \hat{W}_1 + \hat{W}_2 + \hat{W}_3$  with

$$\begin{aligned}\hat{W}_1 f_i(\mathbf{r}) &= \rho_0 \int d^2r' (\sqrt{g(\mathbf{r})} - 1) W(\mathbf{r} - \mathbf{r}') \sqrt{g(\mathbf{r}')} f_i(\mathbf{r}') \\ \hat{W}_2 f_i(\mathbf{r}) &= \rho_0 \int d^2r' W(\mathbf{r} - \mathbf{r}') (\sqrt{g(\mathbf{r}')} - 1) f_i(\mathbf{r}') \\ \hat{W}_3 f_i(\mathbf{r}) &= \rho_0 \int d^2r' W(\mathbf{r} - \mathbf{r}') f_i(\mathbf{r}')\end{aligned}$$

The first two terms turn out to be small because  $\sqrt{g(\mathbf{r})} - 1$  becomes small for large  $r$ . The third term is still large but has the form of a convolution integral, hence it can be easily exponentiated in momentum space. We obtain the following approximate imaginary time propagation operator for small time steps  $\tau$

$$G = e^{-\frac{\tau}{2}[\frac{\hbar^2 k^2}{m} + W(\mathbf{k})]} \mathcal{F} e^{-\frac{\tau}{2}[V(\mathbf{r}) + w_I(\mathbf{r})]} [1 - \tau(\hat{W}_1 + \hat{W}_2)] e^{-\frac{\tau}{2}[V(\mathbf{r}) + w_I(\mathbf{r})]} \mathcal{F}^{-1} e^{-\frac{\tau}{2}[\frac{\hbar^2 k^2}{m} + W(\mathbf{k})]}$$

where we used a symmetric form of the Trotter approximation.  $\mathcal{F}$  denotes the fast Fourier transformation. For this propagator we can use a time step two orders of magnitude larger than for a propagator without the above splitting of  $\hat{W}$  into small and large contributions.

## Appendix B: Phase Boundaries

We use a C-support vector machine [51] to trace the boundaries of the different phases shown in fig. 7. We have trained a classifier for each pair of the three classes ( $j = 1$  for striped liquid,  $j = 2$  for dipolar gas, and  $j = 3$  for homogeneous liquid) The classifiers have the form

$$f_j(\mathbf{x}) = \sum_i y_j^i \alpha_{ij} k(\mathbf{x}, \mathbf{x}^i) + b_j. \quad (\text{B1})$$

where  $k$  is the kernel, which has been chosen to be simply

$$k(\mathbf{x}, \mathbf{x}') = (\gamma \langle \mathbf{x}, \mathbf{x}' \rangle)^d, \quad (\text{B2})$$

where  $\langle \dots \rangle$  denotes the dot product and  $\mathbf{x} = (\theta, C_h)$ . For the upper panel in fig. 7,  $d = 6$ ,  $\gamma = 3.2531$  and  $b_j = \{-27.5267, 56.9545, 23.9379\}$ . The dual coefficients  $y_j^i \alpha_{ij}$  and the support vectors (SV)  $\mathbf{x}^i$  are found in tab. I. Each support vector is used in two classifiers so there are

$y_j^i \alpha_{ij}$						
$j = 1$	0.	0.776	0.	0.	0.	2.607
	6.	0.	6.	6.	2.872	0.
$j = 2$	0.	0.	-3.384			
	0.354	0.770	0.			
$j = 3$	0.	-2.775	-6.	-2.285	-6.	-3.812
	-1.124	0.	0.	0.	0.	0.

	$\theta$	$C_h/r_0$
SV class 1	1.14	0.32
	1.05	0.34
	1.11	0.34
	1.18	0.29
	1.19	0.28
	1.	0.29
SV class 2	1.08	0.38
	1.09	0.39
	1.01	0.31
SV class 3	1.09	0.38
	1.13	0.33
	1.09	0.35
	1.16	0.31
	1.17	0.3
	1.21	0.27

TABLE I. Dual coefficients and support vectors (SV) for the upper panel of fig. 7.

two dual coefficients for each  $\mathbf{x}^i$  (columns in the upper part of tab. I). The phase boundaries between class  $j$  and  $k$  are then obtained imposing the condition

$$f_j(\mathbf{x}) - f_k(\mathbf{x}) = 0. \quad (\text{B3})$$

The classifier was trained with ten-fold cross-validation and a regularization parameter of  $C = 6$ , which avoids over-fitting of the training data.

## Appendix C: Elementary Diagrams

$\theta$	$C_h/r_0$	$\rho_{c/\text{eq}} \cdot r_0^2$	$\Delta e_{\text{ele}}[\%]$
1.08	0.33	0.2023	0.01
1.16	0.33	0.6489	0.93
1.14	0.30	1.00	2.94
1.19	0.28	1.9245	9.31
1.21	0.27	2.4742	13.95
1.21	0.26	2.9948	20.68

TABLE II. Contribution of the elementary diagrams to the total energy  $\Delta e_{\text{ele}}$  in percent. The third column either gives the critical density  $\rho_c$  (rows 1, 3, 4 and 6) or the equilibrium density  $\rho_{\text{eq}}$  (row 2 and 5).

We investigated the influence of elementary diagrams by calculating the energy contribution  $e_{\text{ele}}$  of the lowest order elementary diagram, the four point diagram [45]. We calculate  $e_{\text{ele}}$  using the pair distribution function  $g(x, y)$  of the HNC-EL/0 results, i.e. from the energy optimization without elementary diagrams. This is justified if the contribution of elementary diagrams is small, otherwise elementary diagrams have to be included self-consistently in the optimization. We report the relative

change in energy compared to the HNC-EL/0 result

$$\Delta e_{\text{ele}} = \frac{e_{\text{ele}}}{e + e_{\text{ele}}} . \quad (\text{C1})$$

in tab. II for several values of  $\theta$ ,  $C_h$  and  $\rho_c$  (striped liquid) or  $\rho_{\text{eq}}$  (homogeneous liquid). For systems with  $\rho_0 r_0^2 \lesssim 1$  the lowest order elementary diagram only gives a small contribution and the HNC-EL/0 approximation is justified. However, for larger densities  $\rho_0 r_0^2 \gtrsim 2$  our estimate for the relative energy correction  $\Delta e_{\text{ele}}$  becomes large and the elementary diagrams should be included self-consistently. In this density regime also triplet correlations to the wave function are expected to play a significant role and should be included as well. Both triples and elementaries have been investigated for  $^4\text{He}$  in the past [39].

- 
- [1] L. Chomaz, I. Ferrier-Barbut, F. Ferlaino, B. Laburthe-Tolra, B. L. Lev, and T. Pfau, “Dipolar physics: A review of experiments with magnetic quantum gases,” arXiv preprint arXiv:2201.02672 (2022).
- [2] M. Lu, N. Q. Burdick, S. H. Youn, and B. L. Lev, “Strongly dipolar Bose-Einstein condensate of dysprosium,” *Phys. Rev. Lett.* **107**, 190401 (2011).
- [3] H. Kadau, M. Schmitt, M. Wenzel, C. Wink, T. Maier, I. Ferrier-Barbut, and T. Pfau, “Observing the Rostensweig instability of a quantum ferrofluid,” *Nature* **530**, 194–197 (2016).
- [4] M. Schmitt, M. Wenzel, F. Böttcher, I. Ferrier-Barbut, and T. Pfau, “Self-bound droplets of a dilute magnetic quantum liquid,” *Nature* **539**, 259–262 (2016).
- [5] I. Ferrier-Barbut, H. Kadau, M. Schmitt, M. Wenzel, and T. Pfau, “Observation of quantum droplets in a strongly dipolar Bose gas,” *Phys. Rev. Lett.* **116**, 215301 (2016).
- [6] I. Ferrier-Barbut, M. Schmitt, M. Wenzel, H. Kadau, and T. Pfau, “Liquid quantum droplets of ultracold magnetic atoms,” *J. Phys. Pt. B Atom M. P.* **49**, 214004 (2016).
- [7] I. Ferrier-Barbut, M. Wenzel, M. Schmitt, F. Böttcher, and T. Pfau, “Onset of a modulational instability in trapped dipolar Bose-Einstein condensates,” *Phys. Rev. A* **97**, 011604 (2018).
- [8] L. Chomaz, S. Baier, D. Petter, M. J. Mark, F. Wächtler, L. Santos, and F. Ferlaino, “Quantum-fluctuation-driven crossover from a dilute Bose-Einstein condensate to a macrodroplet in a dipolar quantum fluid,” *Phys. Rev. X* **6**, 041039 (2016).
- [9] F. Wächtler and L. Santos, “Quantum filaments in dipolar Bose-Einstein condensates,” *Phys. Rev. A* **93**, 061603 (2016).
- [10] D. Baillie, R. M. Wilson, R. N. Bisset, and P. B. Blakie, “Self-bound dipolar droplet: A localized matter wave in free space,” *Phys. Rev. A* **94**, 021602 (2016).
- [11] R. Bombin, J. Boronat, and F. Mazzanti, “Dipolar Bose supersolid stripes,” *Phys. Rev. Lett.* **119**, 250402 (2017).
- [12] A. Trautmann, P. Ilzhöfer, G. Durastante, C. Politi, M. Sohmen, M. J. Mark, and F. Ferlaino, “Dipolar quantum mixtures of erbium and dysprosium atoms,” *Phys. Rev. Lett.* **121**, 213601 (2018).
- [13] G. Durastante, C. Politi, M. Sohmen, P. Ilzhöfer, M. J. Mark, M. A. Norcia, and F. Ferlaino, “Feshbach resonances in an erbium-dysprosium dipolar mixture,” *Phys. Rev. A* **102**, 033330 (2020).
- [14] R. N. Bisset, L. A. Peña Ardila, and L. Santos, “Quantum droplets of dipolar mixtures,” *Phys. Rev. Lett.* **126**, 025301 (2021).
- [15] J. C. Smith, D. Baillie, and P. B. Blakie, “Quantum droplet states of a binary magnetic gas,” *Phys. Rev. Lett.* **126**, 025302 (2021).
- [16] J. Léonard, A. Morales, P. Zupancic, T. Esslinger, and T. Donner, “Supersolid formation in a quantum gas breaking a continuous translational symmetry,” *Nature* **543**, 87–90 (2017).
- [17] L. Tanzi, S. M. Roccuzzo, E. Lucioni, F. Famà, A. Fioretti, C. Gabbanini, G. Modugno, A. Recati, and S. Stringari, “Supersolid symmetry breaking from compressional oscillations in a dipolar quantum gas,” *Nature* **574**, 382–385 (2019).
- [18] Y.-C. Zhang, F. Maucher, and T. Pohl, “Supersolidity around a critical point in dipolar Bose-Einstein condensates,” *Phys. Rev. Lett.* **123**, 015301 (2019).
- [19] S. M. Roccuzzo and F. Ancilotto, “Supersolid behavior of a dipolar Bose-Einstein condensate confined in a tube,” *Phys. Rev. A* **99**, 041601 (2019).
- [20] J. Hertkorn, J.-N. Schmidt, F. Böttcher, M. Guo, M. Schmidt, K. S. H. Ng, S. D. Graham, H. P. Büchler, T. Langen, M. Zwerlein, and T. Pfau, “Density fluctuations across the superfluid-supersolid phase transition in a dipolar quantum gas,” *Phys. Rev. X* **11**, 011037 (2021).
- [21] L. Tanzi, J. G. Maloberti, G. Biagioni, A. Fioretti, C. Gabbanini, and G. Modugno, “Evidence of superfluidity in a dipolar supersolid from nonclassical rotational inertia,” *Science* **371**, 1162–1165 (2021).
- [22] L. Santos, G. V. Shlyapnikov, and M. Lewenstein, “Roton-maxon spectrum and stability of trapped dipolar Bose-Einstein condensates,” *Phys. Rev. Lett.* **90**, 250403 (2003).
- [23] D. H. J. O’Dell, S. Giovanazzi, and G. Kurizki, “Rtons in gaseous bose-einstein condensates irradiated by a laser,” *Phys. Rev. Lett.* **90**, 110402/1–4 (2003).

- [24] L. Chomaz, R. M. W. van Bijnen, D. Petter, G. Faraoni, S. Baier, J. H. Becher, M. J. Mark, F. Wächtler, L. Santos, and F. Ferlaino, “Observation of the Roton Mode in a Dipolar Quantum Gas,” *Nat. Phys.* (2018), 10.1038/s41567-018-0054-7.
- [25] G. Natale, R. M. W. van Bijnen, A. Patscheider, D. Petter, M. J. Mark, L. Chomaz, and F. Ferlaino, “Excitation spectrum of a trapped dipolar supersolid and its experimental evidence,” *Phys. Rev. Lett.* **123**, 050402 (2019).
- [26] J.-N. Schmidt, J. Hertkorn, M. Guo, F. Böttcher, M. Schmidt, K. S. H. Ng, S. D. Graham, T. Langen, M. Zwierlein, and T. Pfau, “Roton excitations in an oblate dipolar quantum gas,” *Phys. Rev. Lett.* **126**, 193002 (2021).
- [27] P. B. Blakie, D. Baillie, L. Chomaz, and F. Ferlaino, “Supersolidity in an elongated dipolar condensate,” *Phys. Rev. Research* **2**, 043318 (2020).
- [28] S. Komineas and N. R. Cooper, “Vortex lattices in Bose-Einstein condensates with dipolar interactions beyond the weak-interaction limit,” *Phys. Rev. A* **75**, 023623 (2007).
- [29] M. Wenzel, F. Böttcher, J.-N. Schmidt, M. Eisenmann, T. Langen, T. Pfau, and I. Ferrier-Barbut, “Anisotropic superfluid behavior of a dipolar Bose-Einstein condensate,” *Phys. Rev. Lett.* **121**, 030401 (2018).
- [30] A. Macia, D. Hufnagl, F. Mazzanti, J. Boronat, and R. E. Zillich, “Excitations and stripe phase formation in a two-dimensional dipolar Bose gas with tilted polarization,” *Phys. Rev. Lett.* **109**, 235307 (2012).
- [31] L. Tanzi, E. Lucioni, F. Famà, J. Catani, A. Fioretti, C. Gabbanini, R. N. Bisset, L. Santos, and G. Modugno, “Observation of a dipolar quantum gas with metastable supersolid properties,” *Phys. Rev. Lett.* **122**, 130405 (2019).
- [32] F. Böttcher, J.-N. Schmidt, M. Wenzel, J. Hertkorn, M. Guo, T. Langen, and T. Pfau, “Transient supersolid properties in an array of dipolar quantum droplets,” *Phys. Rev. X* **9**, 011051 (2019).
- [33] L. Chomaz, D. Petter, P. Ilzhöfer, G. Natale, A. Trautmann, C. Politi, G. Durastante, R. M. W. van Bijnen, A. Patscheider, M. Sohmen, M. J. Mark, and F. Ferlaino, “Long-lived and transient supersolid behaviors in dipolar quantum gases,” *Phys. Rev. X* **9**, 021012 (2019).
- [34] P. Ilzhöfer, M. Sohmen, G. Durastante, C. Politi, A. Trautmann, G. Natale, G. Morpurgo, T. Giamarchi, L. Chomaz, M. J. Mark, *et al.*, “Phase coherence in out-of-equilibrium supersolid states of ultracold dipolar atoms,” *Nature Physics* **17**, 356–361 (2021).
- [35] A. Macia, J. Boronat, and F. Mazzanti, “Phase diagram of dipolar bosons in two dimensions with tilted polarization,” *Phys. Rev. A* **90**, 061601 (2014).
- [36] A. Macia, J. Sánchez-Baena, J. Boronat, and F. Mazzanti, “Droplets of trapped quantum dipolar bosons,” *Phys. Rev. Lett.* **117**, 205301 (2016).
- [37] F. Böttcher, M. Wenzel, J.-N. Schmidt, M. Guo, T. Langen, I. Ferrier-Barbut, T. Pfau, R. Bombín, J. Sánchez-Baena, J. Boronat, and F. Mazzanti, “Dilute dipolar quantum droplets beyond the extended Gross-Pitaevskii equation,” *Phys. Rev. Research* **1**, 033088 (2019).
- [38] Y. Kora and M. Boninsegni, “Patterned supersolids in dipolar Bose systems,” *J. Low Temp. Phys.* **197**, 337–347 (2019).
- [39] E. Krotscheck, “Optimal three-body correlations and elementary diagrams in liquid  $^4\text{He}$ ,” *Phys. Rev. B* **33**, 3158 (1986).
- [40] E. Krotscheck, “Theory of correlated basis functions,” in *Introduction to Modern Methods of Quantum Many-Body Theory and their Applications*, Advances in Quantum Many-Body Theory, Vol. 7, edited by A. Fabrocini, S. Fantoni, and E. Krotscheck (World Scientific, Singapore, 2002) pp. 267–330.
- [41] A. Polls and F. Mazzanti, “Microscopic description of quantum liquids,” in *Introduction to Modern Methods of Quantum Many-Body Theory and Their Applications*, Series on Advances in Quantum Many Body Theory Vol.7, edited by A. Fabrocini, S. Fantoni, and E. Krotscheck (World Scientific, 2002) p. 49.
- [42] M. Hebenstreit, M. Rader, and R. E. Zillich, “Dipolar bilayer with antiparallel polarization: A self-bound liquid,” *Phys. Rev. A* **93**, 013611 (2016).
- [43] C. Staudinger, F. Mazzanti, and R. E. Zillich, “Self-bound Bose mixtures,” *Phys. Rev. A* **98**, 023633 (2018).
- [44] E. Feenberg, *Theory of Quantum Fluids* (Academic Press, 1969).
- [45] J. P. Hansen and I. R. McDonald, *Theory of Simple Liquids* (Academic Press, 1986).
- [46] B. E. Clements, H. Forbert, E. Krotscheck, and M. Saarela, “ $^4\text{He}$  on weakly attractive substrates: structure stability, and wetting behavior,” *J. of Low Temp. Phys.* **95**, 849 (1994).
- [47] C. E. Campbell, R. Folk, and E. Krotscheck, “Critical behaviour of liquid  $^4\text{He}$  at negative pressure,” *J. Low Temp. Phys.* **105**, 13 (1996).
- [48] M. Rader, M. Hebenstreit, and R. E. Zillich, “Multicomponent correlated-basis-function method and its application to multilayered dipolar Bose gases,” *Phys. Rev. A* **95**, 033625 (2017).
- [49] L. Castillejo, A. D. Jackson, B. K. Jennings, and R. A. Smith, “Optimal and nearly optimal distribution functions for  $^4\text{He}$ ,” *Phys. Rev. B* **20**, 3631–3640 (1979).
- [50] A. Macia, F. Mazzanti, J. Boronat, and R. E. Zillich, “Microscopic description of anisotropic low-density dipolar Bose gases in two dimensions,” *Phys. Rev. A* **84**, 033625 (2011).
- [51] F. Pedregosa, G. Varoquaux, A. Gramfort, V. Michel, B. Thirion, O. Grisel, M. Blondel, P. Prettenhofer, R. Weiss, V. Dubourg, J. Vanderplas, A. Passos, D. Cournapeau, M. Brucher, M. Perrot, and E. Duchesnay, “Scikit-learn: Machine learning in Python,” *J. Mach. Learn. Res.* **12**, 2825–2830 (2011).
- [52] E. Krotscheck, “Inhomogeneous quantum liquids: Statics, dynamics, and thermodynamics,” in *Microscopic Quantum Many-Body Theories and Their Applications*, Lecture Notes in Physics, Vol. 510, edited by Jesús Navarro and Artur Polls (Springer, 1998) pp. 187–250.
- [53] D. Hufnagl, R. Kaltseis, V. Apaja, and R. E. Zillich, “Roton-roton crossover in strongly correlated dipolar Bose-Einstein condensates,” *Phys. Rev. Lett.* **107**, 065303 (2011).
- [54] D. Hufnagl and R. E. Zillich, “Stability and excitations of a bilayer of strongly correlated dipolar bosons,” *Phys. Rev. A* **87**, 033624 (2013).
- [55] H. F. Trotter, “On the product of semi-groups of operators,” *Proc. Am. Math. Soc.* **10**, 545 (1959).